# Discerning the neutron density distribution of <sup>208</sup>Pb from nucleon elastic scattering

S. Karataglidis<sup>1</sup>, K. Amos<sup>1,2</sup>, B. A. Brown<sup>3</sup>, and P. K. Deb<sup>2</sup>

<sup>1</sup>Theoretical Division, Los Alamos National Laboratory, Los Alamos, New Mexico, 87545

<sup>2</sup>School of Physics, University of Melbourne, Victoria 3010, Australia

<sup>3</sup>National Superconducting Cyclotron Laboratory and Department of Physics and Astronomy,

Michigan State University, East Lansing, Michigan, 48824-1321

(October 26, 2018)

## Abstract

We seek a measure of the neutron density of  $^{208}\text{Pb}$  from analyses of intermediate energy nucleon elastic scattering. The pertinent model for such analyses is based on coordinate space nonlocal optical potentials obtained from model nuclear ground state densities. Those potentials give predictions of integral observables and of angular distributions which show sensitivity to the neutron density. When compared with experiment, and correlated with analyses of electron scattering data, the results suggest that  $^{208}\text{Pb}$  has a neutron skin thickness  $\sim 0.17$  fm.

#### I. INTRODUCTION

Interest in the matter distributions of  $^{208}$ Pb, and its neutron density profile particularly, is quite topical [1]. There is a proposal to measure its neutron root-mean-square (rms) radius at the Jefferson Laboratory [2] from an analysis of parity-violating electron scattering data. In contrast to proton rms radii that are known to within an accuracy  $\sim 0.02$  fm [3], neutron rms radii are less certain.

Recently, the neutron rms radius in  $^{208}\text{Pb}$  was assessed in terms of modern Skyrme-Hartree-Fock (SHF) models [1]. With the Friedman-Pandharipande (FP) neutron equation of state [4] as a constraint, the neutron rms radius in  $^{208}\text{Pb}$  was expected to be  $0.16\pm0.02$  fm larger than the proton value. Previous estimates of this neutron skin,  $S = \sqrt{\langle r_n^2 \rangle} - \sqrt{\langle r_p^2 \rangle}$ , ranged from 0.1 fm to 0.3 fm [2,5]; the lower values favored in general by SHF models, while relativistic mean field models predict values closer to 0.3 fm [6]. Knowledge of the skin thickness in  $^{208}\text{Pb}$  then is a good constraint upon such models of structure [6].

The planned parity-violating electron scattering experiment [2] will only provide information about the neutron rms radius itself. We seek further information and address the question of whether analyses of nucleon scattering data establish a measure of the neutron density distribution in <sup>208</sup>Pb. Hadron scattering data have been analyzed previously to deduce the neutron skin thickness in <sup>208</sup>Pb. The ratio of  $\pi^+$  and  $\pi^-$  reaction cross sections gave  $S = 0.0 \pm 0.1$  fm [7]. Analyses of elastic proton scattering data at 0.8 GeV gave  $0.14 \pm 0.04$  fm [8]. However, a review of the analysis of proton scattering from <sup>40</sup>Ca [9] gave values in the range of -0.4 fm to -0.2 fm for S in that nucleus which are systematically smaller than all theoretical models which give -0.05 fm [10], and suggests that there is a systematic problem in the analysis using phenomenological models of high energy proton scattering data which would affect the extracted S values at the level of  $\sim 0.2$  fm. A more recent analysis of 650 MeV proton scattering data [11] gave  $S = 0.20 \pm 0.04$  fm for <sup>208</sup>Pb while that reaction model gave a result for <sup>40</sup>Ca which is consistent with theoretical predictions. The excitation of the isovector giant dipole resonance in <sup>208</sup>Pb by inelastic alpha scattering [12] was used to deduce  $S = 0.19 \pm 0.09$  fm. These previous analyses, based on phenomenological models, produce a range of results for <sup>208</sup>Pb and suggest that there may be small but systematic errors in those strong interaction models for hadron scattering limiting the accuracy in the extraction of S to  $\sim 0.2$  fm.

Our approach is based on coordinate space nonlocal optical potentials generated by a full folding of realistic effective nucleon-nucleon (NN) interactions with ground state density matrices (termed densities hereafter) of  $^{208}$ Pb. This allows us to distinguish between various model structures, including those of the SHF type proposed by Brown [1], even if two may have the same rms radii. As a calibration of the use of SHF models we consider the elastic scattering from  $^{40}$ Ca as well. Further, as the effective NN interaction is dominated by the isoscalar  $^{3}S_{1}$  channel [13], proton scattering predominantly will probe the neutron density and vice-versa and so we consider both proton and neutron elastic scattering at a given energy seeking as complete a map as possible of the nuclear matter distributions.

## II. NUCLEAR MODELS AND THE MICROSCOPIC OPTICAL POTENTIAL

The model with which predictions of nucleon-nucleus (NA) scattering observables are made has been given in detail in a recent review [13]. Use of the complex, nonlocal, NA optical potentials defined by that model prescription, without localization of the exchange amplitudes, gave predictions of differential cross sections and spin observables that are in good agreement with data from many nuclei ( $^{3}$ He to  $^{238}$ U) and for a wide range of energies (40 to 300 MeV). Crucial to that success was the use of effective NN interactions built upon NN g matrices; solutions of Brueckner-Bethe-Goldstone equations for realistic starting (free) NN interactions. The NA optical potentials result from folding those effective interactions with the densities of the target nucleus. That folding includes the antisymmetrization of the projectile-nucleus wave functions and therefore exchange (knock-out) amplitudes are treated explicitly. Consequently the NA potentials inherently are non-local. The optical potentials that result from that process we term for brevity as g-folding potentials.

Recently, this approach was applied successfully to make predictions of the integral observables of nucleon elastic scattering [14]. Thus, the use of the g-folding optical potentials give good predictions to both angular-dependent and integral observables; a result not guaranteed with the more common phenomenological approaches. Of import, however, is that the level of agreement with data in the g-folding model depends on the quality of the underlying model of structure. We seek to use that dependence as a sensitive evaluation of the densities considered.

Our theoretical density distributions are based upon the Skyrme Hartree-Fock model for  $^{208}\text{Pb}$  with a spherical closed-shell configuration. It was shown in [1] that there is a combination of parameters in the Skyrme Hamiltonian (dominated by the  $x_3$  parameter) which has a strong influence on the neutron skin thickness but which are not well determined by the data on binding energies and charge radii. This combination can be correlated with the pressure in the neutron equation of state at normal nuclear density [1]. It can also be related to the surface symmetry energy [10]. The Skyrme interaction SKX [15] was obtained with a constraint on the neutron equation of state provided by the FP model [4] which constrains the neutron skin in  $^{208}\text{Pb}$  to be  $S=0.16\pm0.02$  fm. The results obtained with the SKX model will be denoted herein by SHF1. If one does not allow for any constraint from a model for the neutron equation of state then a much larger range of S is allowed. In particular, we use a model which is constrained by the same nuclear properties used for SKX but with a value of the parameters which gives S=0.25 fm for  $^{208}\text{Pb}$ . This we denote as SHF2. The densities for  $^{208}\text{Pb}$  obtained from these models, as well as the others considered herein, are shown in Fig. 1.

An initial test of these interactions is provided by the elastic electron scattering data which yields information on the charge density which, in turn, gives information on the proton density. SKX appears to give an excellent reproduction of the charge-density distribution (Fig. 11 of [15]). However, there is some model dependence in the extraction of the charge density from electron scattering data. It is better to compare to a representation which is more closely associated with the actual data – this is the plane-wave transform of the charge density shown in Fig. 2. The experimental form factor is obtained from the charge density distribution given in [3]. Experiment is compared with the SHF1 and SHF2 model results showing a disagreement with data which systematically increases with momentum

transfer. The main feature of the distribution which affects the high-q behavior is the surface thickness. As discussed in [15], the SKX interaction appears to have a surface thickness which is a little sharper than that determined from experiment. We have thus looked at other Skyrme interactions in terms of the data in Fig. 2 and find the older SKM\* interaction [16] is much better than others in this regard. SKM\* appears to achieve this improvement by a decrease in the power of the density,  $\rho^{\alpha}$ , associated with the density-dependent part of the interaction from its value  $\alpha = 1/2$  for SKX to  $\alpha = 1/6$  for SKM\*. Coincidentally, SKM\* predicts a neutron skin of 0.17 fm which is essentially the same as that predicted by SKX (SHF1 model). This is obtained mainly because the  $x_3$  parameter was set to zero by default, since it is not well determined by nuclear data.

The value of  $\alpha$  is also associated with the incompressibility coefficient K for infinite nuclear matter which ranges from K=270 MeV for SKX to K=217 MeV for SKM\*. It was found in [15] that  $\alpha=1/2$  gave the best overall fit with the data set considered and that when  $\alpha$  is decreased (as in the SKXm interaction, which has  $\alpha=1/3$ ) the overall  $\chi^2$  increased mainly because of an increase in the contribution from the single-particle energies. It was also argued in [15] that an improvement in the surface properties may require an additional parameter in the Skyrme Hamiltonian associated with the next order d-wave term in the expansion in terms of the range of the NN interaction. Thus the present models are not perfect but they are good enough for a discussion of the effects of the neutron skin and the surface thickness on the proton and neutron scattering data. We compare results obtained with three Skyrme interactions SHF1 (SKX), SHF2, and SKM\* which will enable us to explore the effect of neutron skin (a comparison of SHF1 and SHF2) with a fixed surface thickness, and surface thickness (a comparison of SHF1 and SKM\*) with a fixed neutron skin.

We compare also with results obtained with the simple harmonic-oscillator radial wave functions for  $^{208}\text{Pb}$  which were used in [13]. Two sets of oscillator parameters were used. For HO1 we use  $\hbar\omega=6.70$  MeV for both protons and neutrons which is chosen to give the rms charge radius of 5.50 fm (a proton rms radius 5.45 fm). HO1 has a neutron rms radius of 5.84 fm. For HO2 the oscillator parameter for neutrons was changed to 7.25 MeV to decrease the rms neutron radius to 5.61 fm so that the neutron skin S=0.16 fm is close to that obtained with SHF1 and SKM\*.

The rms radii from all models of the ground state of  $^{208}\text{Pb}$  considered are listed in Table I. All five give essentially the same radius for the protons but they vary considerably in the radius for the neutrons. The difference between the neutron and proton rms radii given in the last column emphasizes that spread. Note that the HO2 model was chosen to give the same rms radii as those of the SHF1 model. The neutron radius obtained from the SKM\* model is similar to those of the SHF1 and HO2 models. However, as is evident in Fig. 1, each model gives distinctive density distributions. The normalization used is such that their volume integrals equate to the proton and neutron numbers of 82 and 126 respectively. In Fig. 1, the proton density  $\rho_p(r)$  of both the SHF1 and SHF2 models are displayed by the solid curve. The density obtained from the SKM\* model is given by the double-dot-dashed line and exhibits a larger diffuseness compared to the densities of the other Skyrme models. Likewise, both the HO1 and HO2 models have proton densities as given by the dot-dashed curve. These quite distinct shapes nevertheless give the same proton rms radius. However, they differ in the longitudinal electron scattering form factor as shown in Fig. 2.

The five model neutron densities  $\rho_n(r)$  are also shown in Fig. 1. The SHF1 and SHF2 neutron densities are displayed by the solid and dashed lines respectively. They are similar with the SHF2 density having a slightly more diffuse surface region; a property that results in the larger neutron rms radius. The density from the SKM\* model is given by the double-dot-dashed line and, as for the proton density, exhibits a larger diffuseness compared to the densities of the other Skyrme models. The neutron densities of the HO1 and HO2 models are displayed by the dotted and dot-dashed lines respectively. As with their proton densities, the neutron densities of both of these models are enhanced in the nuclear interior over the SHF values. But these HO densities also have increased neutron probability at the surface. Recall that the HO2 model was set to have the same neutron rms radius as the SHF1 prescription.

The SHF (SKX) densities for  $^{40}$ Ca are displayed in Fig. 3. Also displayed therein are the densities from the oscillator model used by Karataglidis and Chadwick [17], for which  $\hbar\omega=10.25$  MeV. In the surface region, the two models predict essentially the same densities. As those densities differ markedly only well within the nuclear volume, we expect influence on scattering primarily at high momentum transfer scattering results at energies for which absorption through the nucleus is not too large. We anticipate differences in cross sections for scattering at energies  $\geq 200$  MeV and at momentum transfer values  $\geq 1$  fm<sup>-1</sup>.

#### III. RESULTS

We have analyzed both proton and (where available) neutron elastic scattering data from  $^{40}$ Ca and  $^{208}$ Pb at 40, 65, and 200 MeV. The choices of energies were predicated in part on the availability of data and of the momentum transfer values at which those data have been measured. In addition our choice was influenced by previous applications of the g-folding potentials with those energies being quite successful [13]. Furthermore, the effective interactions defined for each energy are quite different due to the energy dependence of medium effects in the basic g matrices so that the set of NA scattering results we obtain provide a consistency check on the various models of structure used.

The differential cross sections for 40 MeV proton and neutron elastic scattering from <sup>40</sup>Ca are presented in Fig. 4. Therein, the proton scattering data of Camis *et al.* [18] and the neutron scattering data of de Vito *et al.* [19] are compared to the results of the calculations made using SHF (solid line) and HO (dashed line) models. The SHF and HO model results equally well describe the data, although they underpredict the proton scattering in the regions of the minima. That disagreement may be due to problems in specifying the effective interaction at low energies [20]. However, further comment should await the consideration of the comparisons of 40 MeV proton scattering from <sup>208</sup>Pb. Whatever any deficiency at this energy there may be though does not affect results we find for, and conclusions we may draw from, scattering at 65 and 200 MeV.

The 65 MeV elastic scattering scattering cross sections for <sup>40</sup>Ca are displayed in Fig. 5. Therein, the agreement between the model results and the proton scattering data of Sakaguchi et al. [21] is now very good; much better than that found in Fig. 4. Also, there is a slight preference for the SHF result at larger angles. In the case of the neutron scattering results, both model results agree but underpredict some of the data of Hjort et al. [22]. However, those data are somewhat problematic as concluded from a recent analysis [17] in

which several sets of data were compared with theory at that energy. A new measurement of this cross section is required to resolve any such problem.

It is with 200 MeV scattering from <sup>40</sup>Ca, displayed in Fig. 6, that we observe significant differences between the predictions of scattering made using the SHF and HO models. For proton scattering that is displayed in Fig. 6(a), the SHF model result agrees well with the data of Hutcheon *et al.* [23] (circles) and Seifert *et al.* [24] (squares) and is a significant improvement on the result found using the HO model. This variation concurs with our expectation that the differences between the inner radial densities of the two models of structure would influence the results of scattering calculations at higher energies. Taking the results at all three energies, we believe that the SHF model is the better description of <sup>40</sup>Ca.

We now turn to <sup>208</sup>Pb and consider first the integral observables from nucleon scattering as a test of sensitivity to the matter distributions of <sup>208</sup>Pb. Those integral observables at 40, 65, and 200 MeV are given in Tables II and III and we note that a study of these quantities with two of these structure models has been made recently [14] for energies 10 to 300 MeV. The total reaction cross sections for both proton and neutron scattering from <sup>208</sup>Pb are listed in Table II. Comparing the results of the calculations at both 40 and 65 MeV with the available proton data indicates a preference for both SHF, the SKM\*, and HO2 models of the ground state density. However, comparing the model results of the neutron total reaction cross section with the available evaluated data at those energies [25] gives a preference for the Skyrme models only. The predicted proton and neutron total reaction cross sections at 200 MeV vary sufficiently that their measurements would be desirable.

The results of our calculations for the total neutron cross sections are given for the three energies in Table III and are compared with the data of Finlay et al. [26]. For 40 MeV the Skyrme models are preferred, although all results overestimate the measured value. At 65 MeV the Skyrme model results agree well with the data, the SKM\* model result doing best of all, and do better than both HO predictions. This is not the case at 200 MeV, where all results predict the measured value reasonably well. While these total reaction and total cross section results together indicate a preference for the Skyrme models, we need additional evidence. We consider then the angular distributions of each scattering.

The differential cross sections for the scattering of 40, 65 and 200 MeV nucleons from <sup>208</sup>Pb are presented in Figs. 7, 8, and 9 respectively. At 40 MeV, proton elastic scattering is shown in Fig. 7 and evidently there is little if any differentiation between the SHF1, SHF2, and SKM\* model results. They both compare well with the data of Blumberg *et al.* [27]. Note, however, that both SHF and the SKM\* calculated results agree much better with the data than do those found using the HO models of structure. The quality of reproduction of the data in this case is in stark contrast to what we found at 40 MeV with <sup>40</sup>Ca. If that is to remain a problem with specification of the effective interaction then it seems to be a nucleus-dependent effect. In the case of neutron scattering, the results of all model calculations agree quite well with the data of de Vito *et al.* [19]. The results for <sup>208</sup>Pb are more distinctive than those for <sup>40</sup>Ca at this and other energies, but so are the distinctions between the model proton densities for both nuclei. However, these results indicate that while the nucleon densities in <sup>208</sup>Pb are better described by the SHF and SKM\* models nucleon scattering at this energy is largely sensitive to the surface properties only. Only in the surface are the proton densities still sufficiently similar for neutron scattering results of

all models to be as alike as they are.

Recall that the integral observables given in Table II make preference to the SHF and SKM\* models of the density. Similar preference is indicated by the differential cross sections for 65 MeV scattering that are displayed in Fig. 8. Considering the neutron scattering first, all models give similar results in good agreement with the data of Ibaraki et al. [28], although above 40° the SHF and SKM\* model results clearly do better. For proton scattering, the SHF and SKM\* models are both in good agreement with each other and with the data and differ only slightly from those of the HO models. As for 40 MeV scattering, the integral observables at 65 MeV concur with these findings that favor the Skyrme models of the density.

The differential cross sections for 200 MeV nucleon scattering from <sup>208</sup>Pb are shown in Fig. 9. In this case only 200 MeV proton scattering data exist [23] for comparison with our predictions. Nevertheless, that comparison confirms the findings from analyses of the lower energy data, namely that the SHF and SKM\* models are the better descriptions of the densities of <sup>208</sup>Pb. In addition, however, some discrimination between the three Skyrme model results is evident at this energy. Of the three Skyrme models, the SKM\* model result agrees best of all with the data while the SHF1 does worst. Given that the rms radii from these two models are very similar, the marked difference indicates a sensitivity to the diffuseness in the density. At this energy, unlike those at lower energies, the neutron scattering results show marked differences between the SHF and HO calculations. Again, we expect that this is due to the scattering of the higher energy probe being more influenced by the bulk nuclear medium properties of the densities. Consequently, a measurement of the 200 MeV neutron elastic scattering, angular distribution and associated integral observables, is certainly desirable.

### IV. CONCLUSIONS

The distinctions between the predictions of nucleon scattering from <sup>208</sup>Pb at these three energies, and found with the set of five model structures used, suffice to select that which most likely prescribes the actual matter densities of the nucleus. A similar conclusion is reached for <sup>40</sup>Ca for the models considered herein. Specifically we contend that the use of q-folding potential model calculations can differentiate between different model structures of the neutron density so as to pin down the neutron rms radius far better than has been possible in the past. As well the process gives a good appraisal of the actual density distribution. For <sup>208</sup>Pb in particular, our analyses indicate that the SKM\* model gives the best representation of the density. Together with analyses of the longitudinal elastic electron scattering form factor it suggests a neutron skin thickness for <sup>208</sup>Pb of 0.17 fm; a value consistent with expectations of the SHF1 model nucleus, which is constrained by the FP neutron equation of state. The only difference between the two models is that of a larger diffuseness for the SKM\* model, accounting for both the agreement between the results and data for both nucleon and electron scattering. This would suggest a need to extend the SKX models to predict a larger diffuseness, for example, by the addition of a d-wave term in the Skyrme Hamiltonian.

One should also note that while a measurement of the skin thickness as proposed in the experiment for the Jefferson Laboratory [2] is important, that quantity is a volume property

of the nucleon distributions. Other information is required to specify a more complete picture of the neutron density. From our studies it seems that simultaneous analyses of angular and integral observables are relevant. Given that the HO2, SHF1, and SKM\* models of structure we have used predict essentially the same skin thickness for  $^{208}$ Pb but give significantly different predictions when used to generate NA g folding optical potentials for the nucleon scattering, as well as electron scattering form factors, analyses of complementary nucleon and electron scattering data permit one to discern such finer details of densities.

This work was supported in part by a grant from the Australian Research Council, U.S. National Science Foundation grants no. PHY-9605207 and PHY-0070911, and DOE Contract no. W-7405-ENG-36. Two of us (S.K. and K.A.) would like to thank the National Superconduncting Cyclotron Laboratory of Michigan State University for their kind hospitality during part of this work, while another one of us (K.A.) would like to thank the Theoretical Division of the Los Alamos National Laboratory for its similar kind hospitality.

## REFERENCES

- [1] B. A. Brown, Phys. Rev. Lett. 85, 5296 (2000).
- [2] Jefferson Laboratory Experiment E-00-003, spokespersons R. Michaels, P. A. Souder, and G. M. Urciuoli.
- [3] G. Fricke et al., At. Data Nucl. Data Tables 60, 177 (1995).
- [4] B. Friedman and V. R. Pandharipande, Nucl. Phys. A361, 502 (1981).
- [5] K. Pomorski, P. Ring, G. A. Lalazissis, A. Baran, Z. Lojewski, B. Nerlo-Pomorska, and M. Warda, Nucl. Phys. A624, 349 (1997).
- [6] S. Typel and B. A. Brown, Phys. Rev. C 64, 027302 (2001).
- [7] B. W. Allardyce et al., Nucl. Phys. **A209**, 1 (1973).
- [8] G. W. Hoffmann et al., Phys. Rev. C 21, 1488 (1980).
- [9] L. Ray, G. W. Hoffmann, and W. R. Coker, Phys. Rep. **212**, 223 (1992).
- [10] S. Stringari and E. Lipparini, Phys. Lett. **117B**, 141 (1982).
- [11] V. E. Starodubsky and N. M. Hintz, Phys. Rev. C 49, 2118 (1994).
- [12] A. Krasznahorkay, A. Balanda, J. A. Bordewijk, S. Brandenburg, M. N. Harakeh, N. Kalantar-Nayestanaki, B. N. Nyakó, J. Timár, and A. van der Woude, Nucl. Phys. A567, 521 (1994).
- [13] K. Amos, P. J. Dortmans, H. V. von Geramb, S. Karataglidis, and J. Raynal, Adv. in Nucl. Phys. 25, 275 (2000).
- [14] P. K. Deb, K. Amos, S. Karataglidis, M. B. Chadwick, and D. G. Madland, Phys. Rev. Lett. 86, 3248 (2001).
- [15] B. A. Brown, Phys. Rev. C 58, 220 (1998).
- [16] J. Bartel, P. Quentin, M. Brack, C. Guet, and H.-B. Hakansoon, Nucl. Phys. A386, 79 (1982).
- [17] S. Karataglidis and M. B. Chadwick, Phys. Rev. C 64, 111111 (2001).
- [18] R. H. McCamis et al., Phys. Rev. C 33, 1624 (1986).
- [19] R. P. de Vito, S. M. Austin, W. Sterrenburg, and U. E. P. Berg, Phys. Rev. Lett. 47, 628 (1981).
- [20] P. K. Deb, K. Amos, and S. Karataglidis, Aust. J. Phys. 53, 767 (2000).
- [21] H. Sakaguchi, M. Nakamura, K. Hatanaka, A. Goto, T. Noro, F. Ohtani, H. Sakamoto, H. Ogawa, and S. Kobyashi, Phys. Rev. C 26, 944 (1982).
- [22] E. L. Hjort, F. P. Brady, J. L. Romero, J. R. Drummond, D. . S. Sorenson, J. H. Osborne, B. McEachern, and L. F. Hansen, Phys. Rev. C 50, 275 (1994).
- [23] D. A. Hutcheon *et al.*, Nucl. Phys. **A483**, 429 (1988).
- [24] H. Seifert *et al.*, Phys. Rev. C **47**, 1615 (1993).
- [25] M. B. Chadwick et~al., Nucl. Sci and Eng. **131**, 293 (1999).
- [26] R. W. Finlay, W. P. Abfalterer, G. Fink, E. Montei, T. Adami, P. W. Lisowski, G. L. Morgan, and R. C. Haight, Phys. Rev. C 47, 237 (1993).
- [27] L. N. Blumberg, E. E. Gross, A. van der Woude, A. Zucker, and R. H. Bassel, Phys. Rev. 147, 812 (1966).
- [28] M. Ibaraki, M. Baba, T. Miura, Y. Hirasawa, Y. Nauchi, H. Makashima, S. Meigo, O. Iwamoto, and S. Tanaka, Nucl. Instrum. Meth. in Phys. Res. A446, 536 (2000).
- [29] R. F. Carlson, A. J. Cox., J. R. Nimmo, N. E. Davison, S. A. Elbakr, J. L. Horton, A. Houdayer, A. M. Sourkes, W. T. H. van Oers, and D. J. Margaziotis, Phys. Rev. C 12, 1167 (1975).

- [30] A. Ingemarsson  $et\ al.$ , Nucl. Phys. **A653**, 341 (1999).
- [31] H. de Vries, C. de Jager, and C. de Vries, At. Data Nucl. Data Tables 36, 495 (1987).

## **TABLES**

TABLE I. Root-mean-square radii (in fm) for protons  $(r_p)$  and neutrons  $(r_n)$  in <sup>208</sup>Pb. The models are as defined in the text.

Model	$r_p$	$r_n$	$r_n - r_p$
HO1	5.45	5.83	0.38
HO2	5.45	5.61	0.16
SHF1	5.45	5.61	0.16
SHF2	5.45	5.70	0.25
SKM*	5.45	5.62	0.17

TABLE II. Total reaction cross sections (in barn) of nucleon scattering from  $^{208}$ Pb. The models used are as specified in the text.

40 MeV		65 MeV		200 MeV		
Model	proton	neutron	proton	neutron	proton	neutron
HO1	2.07	2.69	2.11	2.32	1.79	1.77
HO2	1.95	2.62	2.00	2.27	1.71	1.73
SHF1	1.89	2.51	1.99	2.19	1.68	1.69
SHF2	1.95	2.55	2.03	2.22	1.72	1.71
$SKM^*$	1.92	2.54	2.01	2.21	1.69	1.70
$\operatorname{Expt}$	$2.01 \pm 0.04$ [29]	2.50 [25]	$2.02 \pm 0.06$ [30]	2.20 [25]		

TABLE III. Total cross sections (in barn) of neutron scattering from  $^{208}{\rm Pb}.$  The models used are as specified in the text.

Model	$40~{ m MeV}$	65 MeV	$200~{ m MeV}$
HO1	5.10	4.86	3.04
HO2	4.94	4.72	2.97
SHF1	4.63	4.61	2.94
SHF2	4.71	4.67	2.94
$SKM^*$	4.69	4.63	2.96
Expt [26]	$4.392 \pm 0.001$	$4.634 \pm 0.001$	$2.990 \pm 0.003$

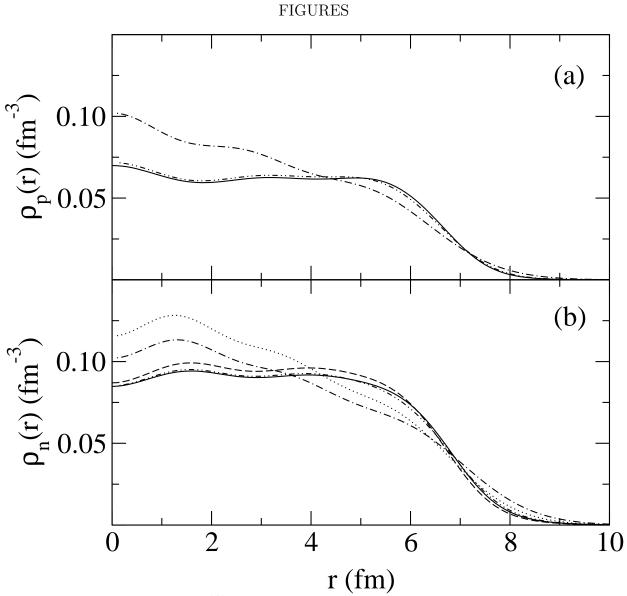


FIG. 1. Nucleon densities in  $^{208}$ Pb. The solid and dot-dashed curves in the proton densities  $\rho_p$  portray both SHF and both HO models respectively. The neutron densities  $\rho_n$  given by the solid, dashed, dotted, and dot-dashed lines portray respectively the SHF1, SHF2, HO1, and HO2 models. The double-dot-dashed line in each case denotes the density obtain from the SKM\* model.

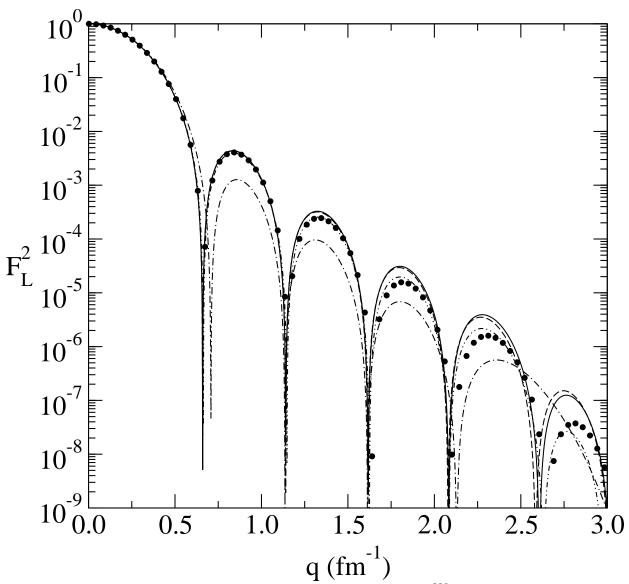


FIG. 2. Longitudinal elastic electron scattering form factor for <sup>208</sup>Pb. The data [31] are compared to the results of the calculations made using the SHF1, SHF2, and SKM\* models portrayed by the solid, dashed, and double-dot-dashed lines, respectively. The oscillator result is portrayed by the dot-dashed line.

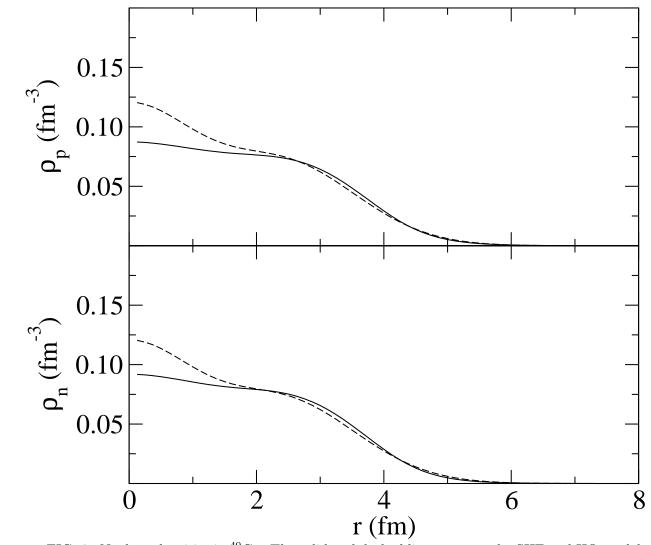


FIG. 3. Nucleon densities in  $^{40}$ Ca. The solid and dashed lines portray the SHF and HO models respectively.

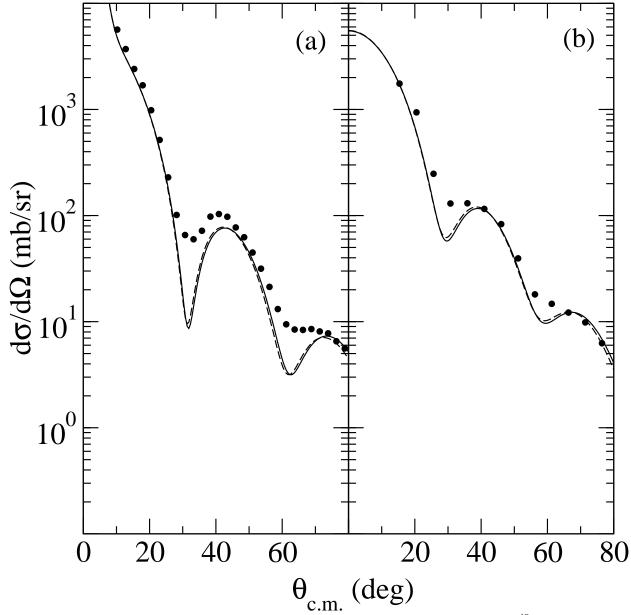
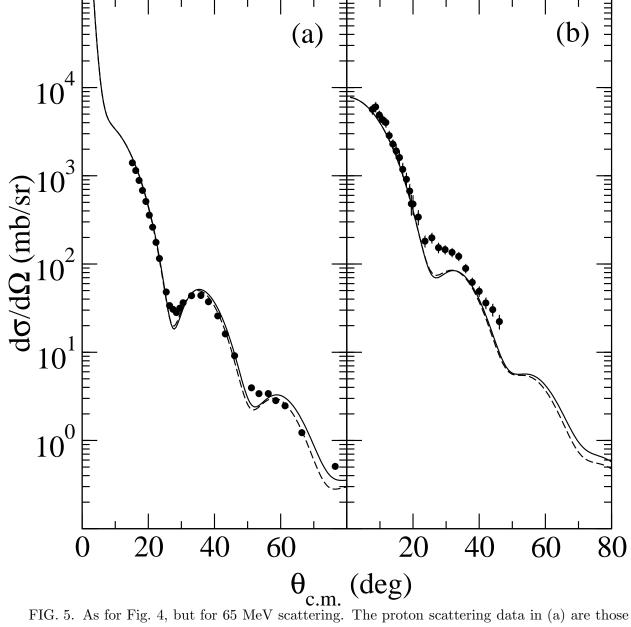
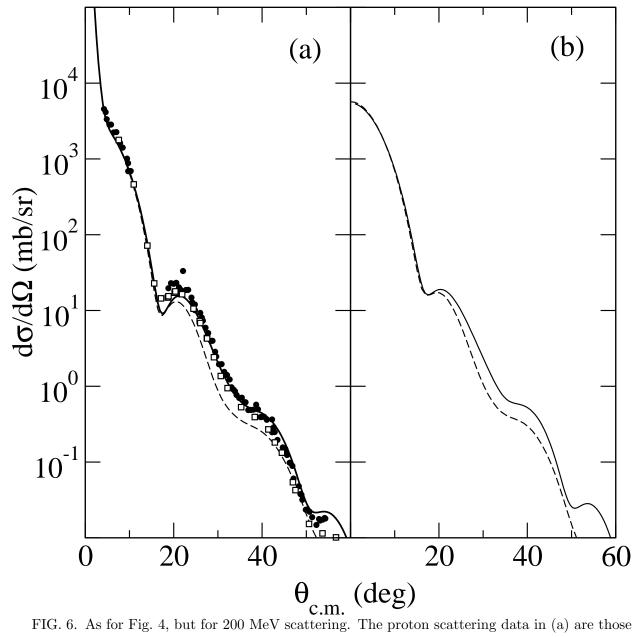


FIG. 4. Differential cross sections for 40 MeV nucleon elastic scattering from <sup>40</sup>Ca. The proton scattering data of Camis *et al.* [18] are compared in (a) with the results of the calculations made as defined in the text. In (b), the neutron scattering data of de Vito *et al.* [19] are compared with the results of equivalent calculations.



of Sakaguchi et al. [21], while the neutron scattering data in (b) are those of Hjort et al. [22].



of Hutcheon et al. [23] (circles) and Seifert et al. [24] (squares).

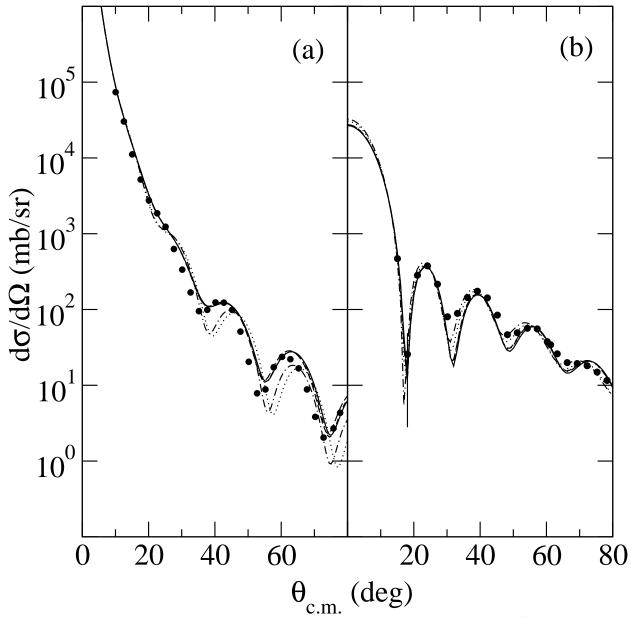
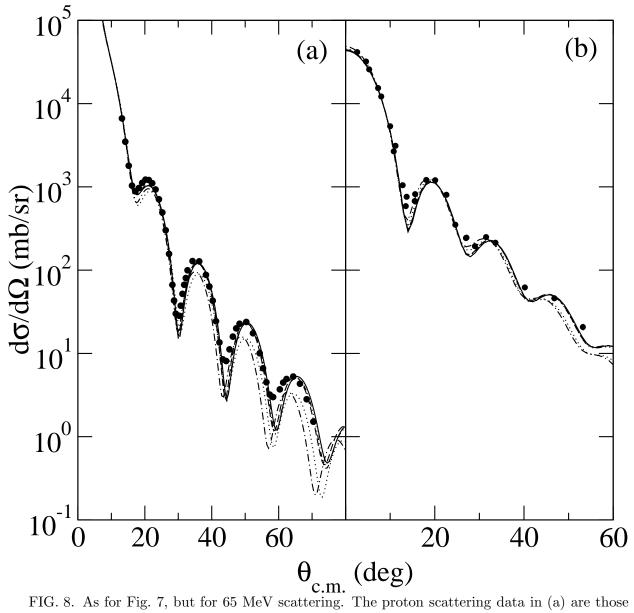
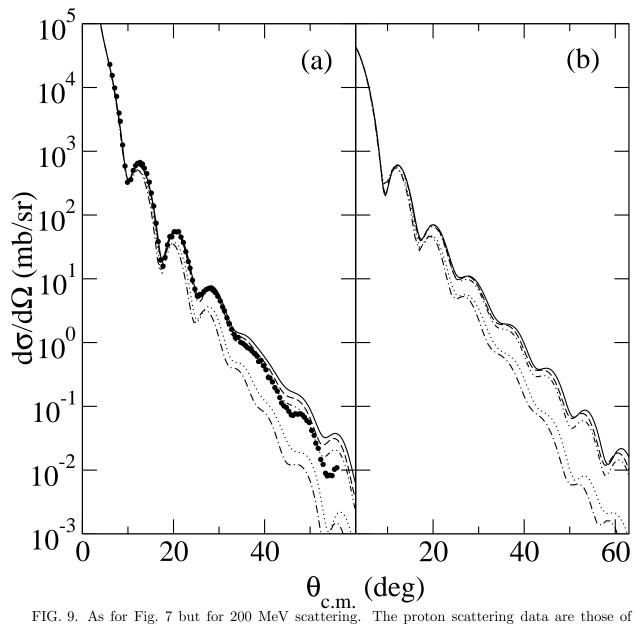


FIG. 7. Differential cross sections for 40 MeV nucleon elastic scattering from <sup>208</sup>Pb. The proton scattering data of Blumberg *et al.* [27] are compared in (a) to the results from the SHF1 and SHF2 models (solid and dashed lines respectively), the SKM\* model (double-dot-dashed line), and to the results of the HO1 and HO2 models (dot-dashed and dotted lines respectively). The neutron scattering data of de Vito *et al.* [19] are compared to the results of those models as defined in (a).



of Sakaguchi et al. [21], while the neutron scattering data in (b) are those of Ibaraki et al. [28].



Hutcheon et al. [23].